Interface effects in plasmon-enhanced second-harmonic generation from self-assembled multilayer films

Kai Chen,[1] Cemil Durak,[1] Akhilesh Garg,[2] Charles Brands,[1] Richey M. Davis,[2] James R. Heflin,[1] and Hans D. Robinson[1,*]

[1]*Department of Physics, Virginia Tech, Blacksburg, Virginia 24061, USA*
[2]*Department of Chemical Engineering, Virginia Tech, Blacksburg, Virginia 24061, USA*
[*]*Corresponding author: hansr@vt.edu*

Received July 1, 2009; accepted November 5, 2009;
posted November 19, 2009 (Doc. ID 113597); published December 24, 2009

We have compared the plasmonic enhancement of second-order nonlinear optical (NLO) properties in two types of ionic self-assembled multilayer (ISAM) films combined with Ag nanoparticles fabricated using nanosphere lithography (NSL). The light-concentrating properties of the Ag particles lead to a marked increase in the NLO efficiencies of thin ISAM films. The induced enhancement is found to be much larger in conventional ISAM films than in films made with the hybrid covalent ISAM technique (HCISAM), even though the latter have a significantly larger intrinsic bulk second-order nonlinear susceptibility ($\chi^{(2)}$). The plasmonic enhancement of NLO effects is shown to be primarily an interface effect due to the short decay length of the plasmon modes. The importance of interface effects in the films has been investigated by surrounding thin ISAM and HCISAM films with NLO-inactive buffer layers, which confirmed the important role played by the interfaces, particularly for the HCISAM films.

OCIS codes: 160.4236, 160.4330, 190.4350, 190.4710, 240.6680, 310.6628.

1. INTRODUCTION

Second-order nonlinear optical (NLO) materials have wide applications as electro-optic modulators, optical switches, and other key components in current telecommunication networks. The materials currently in use for these applications are inorganic ferroelectrics such as lithium niobate and beta barium borate, which are difficult and expensive to fabricate in the required quality and size. Lower cost organic alternatives contending to replace these materials include ionic self-assembled multilayer (ISAM) films, which can exhibit high $\chi^{(2)}$ values when properly designed and fabricated [1–4].

ISAM films are fabricated through layer-by-layer (LbL) deposition [5] in which a charged substrate is alternately immersed in solutions of oppositely charged polyelectrolytes. Specifically, when a negatively charged substrate is immersed in a polycation solution, a thin layer of the polymer is absorbed on the surface due to electrostatic attraction, creating a positively charged surface. This charge reversal makes it possible to deposit a polyanion layer through the same procedure. This process can be repeated as many times as desired to form films with arbitrary thickness and to have control over film properties at the molecular level. For example [2], using a polyanion with an NLO active chromophore side group results in an ISAM film with significant bulk $\chi^{(2)}$, as illustrated in Fig. 1(a). This occurs because the kinetics of the LbL process causes the majority of the chromophores to orient towards the surface so that the film acquires the polar order necessary for a nonzero $\chi^{(2)}$. The order is however far from perfect, with a significant number of chromophores oriented in the opposite direction, which reduces the NLO efficiency of the film. To overcome this, our group has previous developed a method for depositing what we will refer to as hybrid covalent ISAM (or HCISAM) films, which results in greater polar order and therefore significantly larger $\chi^{(2)}$ values. Here, the polyanion is replaced by an NLO active monomer, which is covalently rather than electrostatically bound to the underlying polycation layer, as shown in Fig. 1(b). The following polycation layer then binds electrostatically to the ionic groups of the monomer exposed at the surface [4]. Using the HCISAM approach, a $\chi^{(2)}_{zzz}$ of 50×10^{-9} electrostatic unit (esu) and an electro-optic coefficient r_{33} of 14 pm/V have been achieved. These values have remained unchanged at room temperature for more than two years and for 24 h at 150 °C [3].

Our group has also recently demonstrated a novel way of increasing the second-order NLO response of ISAM films by several orders of magnitude [6]. This was accomplished by plasmonic enhancement achieved by depositing triangular Ag nanoparticles (NPs) on ISAM films using nanosphere lithography (NSL) [7,8]. We denote these films as NP-ISAM films. We showed that the second-harmonic generation (SHG) conversion efficiency of a thin NLO active ISAM film could be enhanced by as much as 1600 times due to the localized surface plasmon resonances associated with the Ag nanoparticles. These arise when an electromagnetic (EM) field at optical frequencies interacts with the conduction electrons in the metal NPs. Under resonant conditions, this gives rise to collective oscillations in the conduction electrons at the frequency of

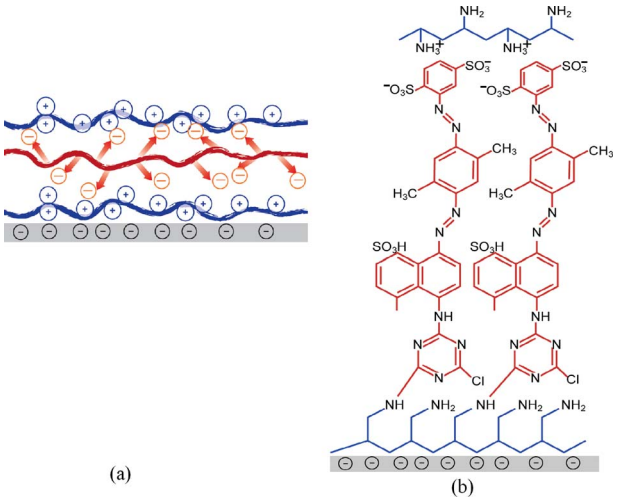

Fig. 1. (Color online) Illustration of the structures of (a) ISAM films, where cationic and anionic polyelectrolytes are arranged in a layered structure, and (b) HCISAM films, where the cationic layer consists of monomers (in this case Procion Brown) that are covalently bound to the underlying polycation (PAH).

the incident light. The nanoparticles then act to concentrate the incoming light into "hot spots," regions a few nanometers thick located at sharp corners or narrow gaps on the surface of the nanoparticles. At the hot spots of a NP, the local EM field intensity can reach up to 10^4 times the intensity of the incident light [9]; even higher values are seen in composite nanostructures [10,11]. Since the efficiency of second-order NLO effects such as SHG increases with the EM field intensity, the combination of NLO materials with Ag nanoparticles can enhance the second-order NLO responses by several orders of magnitude beyond what is seen in the unmodified films. In the case of nonlinear phenomena, the increase in the response in these hot spots results in a corresponding net increase in the total signal despite the decrease in the EM field intensity in other regions of the material. Other workers have used this same principle in different configurations, achieving similarly impressive results [12–15].

In this paper, we study the combination of plasmonic nanoparticles with HCISAM films as the next logical step towards high-$\chi^{(2)}$ ISAM films. Despite the 25 times larger $\chi^{(2)}$ values of the HCISAM films, the SHG conversion efficiency is larger for plasmonically enhanced ISAM films than for plasmonically enhanced HCISAM films. This demonstrates that the plasmonic enhancement is primarily an interface effect. The interface SHG of ISAM and HCISAM films are thus investigated in detail.

2. EXPERIMENTAL

Poly(allylamine hydrochloride) (PAH) ($M_w \sim 70$ kDa, Aldrich) was used as polycation in all of the samples. Poly(1-[p-(3′-carboxy-4′-hydroxyphenylazo)benzenesulonamido]-1,2-ethandiyl, sodium salt) (PCBS) purchased from Aldrich was used as polyanionic chromophore. Purified Procion Brown (PB) was used as the reactive monomeric chromophore in the HCISAM films. Poly(acrylic acid) (PAA) was used as polyanion in the NLO inactive buffer layers. The films were deposited on glass microscope slides that were cleaned using the RCA cleaning procedure [16] and stored in de-ionized (DI) water until used. Silver pellets (99.99% pure) were purchased from Kurt J. Lesker. Carboxyl functionalized polystyrene latex nanospheres (Invitrogen) with a diameter of 780 nm were used in the NSL procedure by which the Ag NPs were fabricated [6].

ISAM films were deposited on glass slide substrates with a StraoSequence Mark VI robotic deposition system (nanoStrata Inc.). Table 1 displays the deposition parameters for ISAM (PAH/PCBS) and HCISAM (PAH/PB) films. The Ag nanoparticles were deposited on top of the ISAM films using NSL with the thickness (or height) of the nanoparticles at 50 nm. Convective self-assembly [17] was used to ensure that the NSL generated large area coverage of uniform nanospheres. A Varian Cary 5000 spectrometer was used to measure the absorption spectra of the samples at normal incidence.

The SHG measurements were taken using a Spectra-Physics Q-switched 10 Hz Nd:YAG laser with a fundamental wavelength of 1064 nm and pulse width of 11 ns. All of the SHG data were taken with a p-polarized incident beam and collected by a Hamamatsu R1924 photomultiplier tube (PMT) in transmission geometry. SHG measurements were made at incident angles between 40° and 50°. The SHG exhibits a relatively weak angular dependence [6] for the NP-ISAM films, while regular fringes are observed from the ISAM and HCISAM films.

3. NANOPARTICLE ENHANCED ISAM FILMS

To compare the effects of adding Ag NPs to ISAM and HCISAM films, four sets of samples were fabricated. Each set consisted of 10 to 12 films where the thickness was varied between 1 and 40 bilayers. Two of the sets were fabricated by conventional LbL growth using PAH and PCBS as the constituents. The other two sets consisted of PAH/PB HCISAM films. In each material system, one set of films was decorated with Ag nanoparticles formed by nanosphere lithography, while the other was left unmodified.

Figure 2 shows a representative extinction spectrum of a NP-ISAM sample, consisting of a 2-bilayer PAH/PCBS ISAM film and 50-nm-thick Ag nanoparticles. Three plasmon modes are excited in the nanoparticles as evidenced by the three major peaks in the spectrum. The dipole-like mode is the dominant resonance with a peak around 1020 nm, which can be tuned by changing the thickness of the Ag nanoparticles [7,8]. In our case, 50 nm is chosen

Table 1. Deposition Conditions for PAH/PCBS and PAH/PB ISAM Films

	PAH/PCBS Film		PAH/PB Film	
	PAH	PCBS	PAH	PB
Concentration (monomer)	10 mM	10 mM	10 mM	5 mg/ml
pH	7	7	7	10.5
Deposition time (minutes)	2	2	2	5
Salts (NaCl)	0	0	0	0.5 M

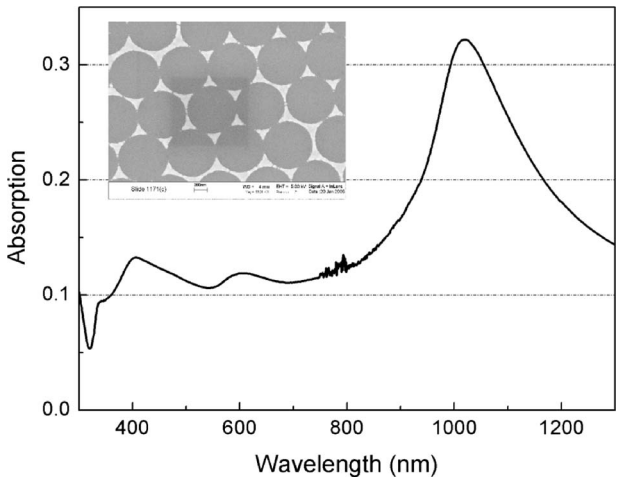

Fig. 2. Absorption spectrum of a 2-bilayer PAH/PCBS ISAM film decorated with triangular Ag nanoparticles fabricated through nanosphere lithography (shown in inset). The noise around 800 nm is due the change of gratings and detectors inside the spectrometer.

to let the dipole resonance overlap with the 1064 nm laser wavelength used in our SHG measurements. By overlapping the plasmon resonance peak with the excitation wavelength, we ensure the maximum enhancement in SHG efficiency as discussed above. The spectral position of the dipole resonance peak varies a little from sample to sample, but always lies in the approximately 980 nm–1080 nm wavelength range, which provides a good overlap with the excitation wavelength.

SHG data from all four sets of samples are plotted in Fig. 3. The SHG intensity from Ag nanoparticles deposited directly on glass is also shown as a reference. There are several points worthy of note in these data. First, for the NP-PCBS films, an SHG efficiency enhancement of ~1400 times for 3-bilayer samples is obtained, consistent with our previous study [6]. Second, one would generally expect the SHG signal from an ISAM film to increase as the square of the film thickness, but this is not seen in our data. For the unmodified films, a quadratic SHG intensity dependence eventually prevails, but only for films thicker

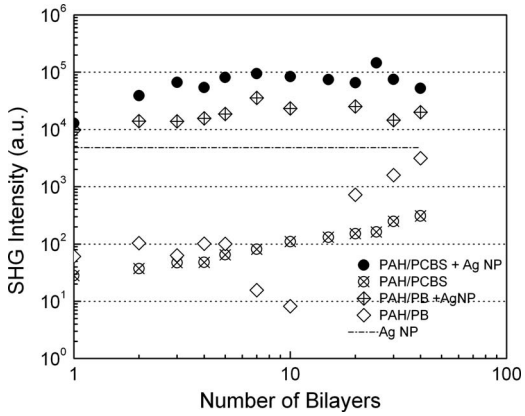

Fig. 3. SHG intensity as a function of film thickness for conventional PAH/PCBS and PAH/PB films (crossed circles and empty diamonds, respectively) and for the same films as modified by Ag nanoparticles (solid circles and crossed diamonds). The dash-dotted line indicates SHG intensity from Ag nanoparticles in the absence of an ISAM film.

than 10 bilayers. Thin PAH/PCBS films show an SHG signal that grows with thickness, but much slower than for thicker films, while the SHG signal from thin PAH/PB films actually decreases with thickness for the first ~10 bilayers. These effects are due to the presence of significant SHG from the films' interfaces, as will be discussed below. The amount of interface SHG is irrespective of film thickness, so we can neglect it for thick ISAM films, even while it dominates for thin ones. The difference in behavior between the two materials systems can be explained by differences in the relative phase between the interface and bulk SHG. As shown below, in the PAH/PCBS films the two are in phase, while in PAH/PB films they are opposite in phase. This leads to a near cancellation of the SHG signal in PAH/PB films that are between 7 and 10 bilayers thick, but not in the PAH/PCBS films.

For the nanoparticle decorated films, we see that the SHG signal is roughly constant for films thicker than two bilayers. This occurs because the decay length of the plasmon resonances away from the NPs is only a few nm. Consequently, only the top few bilayers of the films benefit from plasmonic enhancement, and increasing film thickness therefore does not lead to an increase in SHG intensity. Since the interface SHG is dominant in thin ISAM and HCISAM films, we can conclude that plasmonic enhancement of the NLO response is primarily an interface effect, and bulk $\chi^{(2)}$ is not necessarily a good indicator of how a film will respond when combined with metal NPs.

Finally, the plasmonic enhancement of the SHG signal from for the 3-bilayer NP-PAH/PB film is only ~200 times, and the film is actually a less efficient emitter of SHG radiation than the corresponding NP-PAH/PCBS film. At large bilayer numbers for the unmodified films, the SHG intensity is much larger for PAH/PB than for PAH/PCBS, as expected due to larger $\chi^{(2)}$ value. Since the plasmon resonances primarily enhance the interface $\chi^{(2)}$ of the films, we must consider the differences in interface properties between the PAH/PB and PAH/PCBS films in order to explain these observations. As explained in more detail below, it is likely that the PAH/PB–air interface is more susceptible to disruption than the PAH/PCBS–air interface. The Ag nanoparticles are deposited by electron-beam evaporation, which is a fairly severe process. The organic films are impacted by hot, fast-moving metal atoms, easily capable of rearranging the chromophores at the surface.

4. INTERFACE EFFECTS

Since interface effects are critical to the NLO response of plasmonically enhanced ISAM films, we have fabricated a set of samples with the purpose of separating the contributions of each interface and the bulk to the total SHG signal. This is accomplished by fabricating NLO-inactive buffer layer(s) above and/or below the NLO-active film. Each buffer consists of 10 PAH/PAA bilayers and has similar dielectric and other properties as the NLO-active films. The buffer films are NLO-inactive since they do not possess any of the conjugated bonds responsible for large nonlinearities in organic molecules. The buffer films remove the majority of the interface dipoles, create a less

sharp surface, and thereby virtually eliminate the SHG signal from the adjacent interface. This is demonstrated by the data in Fig. 4, which plots the square root of the SHG intensity generated by a series of PAH/PCBS films, fabricated with and without ten buffer layers, as a function of the number of NLO-active bilayers. The slopes of the curves are constant and identical in both cases, stemming from the bulk contribution to SHG. The y intercept of the series without buffer layers indicates the contribution of the interfaces to SHG, and when buffer layers are added, this contribution goes to zero.

Four combinations of buffers and NLO-active films were fabricated: film only, buffer–film (i.e., the buffer is located below the film), film–buffer, and buffer–film–buffer, as is indicated in Fig. 5. The NLO active film was either one or three bilayers thick and consisted either of a PAH/PCBS ISAM film or a PAH/PB HCISAM film for a total of 16 different samples. Peak optical absorbance (at 365 nm for PCBS ISAM films and 460 nm for PB HCISAM films) and SHG efficiency were measured for each sample, and the data are shown in Fig. 6. In this case, the SHG exhibits Maker-like fringes due to interference between the films on opposite sides of the substrate, [3] and the peak intensity near an incident angle of 45° is reported in the figure. As before, the square root of SHG is used as a measure of the second-order NLO properties [the square root of SHG intensity is proportional to the $\chi^{(2)}$ of the film, and is plotted in Figs. 6(c) and 6(d)]. The absorbance [Figs. 6(a) and 6(b)] is proportional to the surface density of the NLO chromophore, which will vary from sample to sample. The square root of the SHG intensity divided by the absorbance is a figure of merit for the films, indicating the NLO efficiency of the film per chromophore and is plotted in Figs. 6(e) and 6(f).

Considering first the absorption data, we first note that the 3-bilayer films contain, not surprisingly, more chromophores than the 1-bilayer films. More interestingly, the films that have a buffer at the bottom (buffer–film and buffer–film–buffer) consistently have larger absorption than those where the NLO active layers are fabricated directly on the glass substrate. This is true for all samples, but particularly noticeable in the 1-bilayer PAH/PB film.

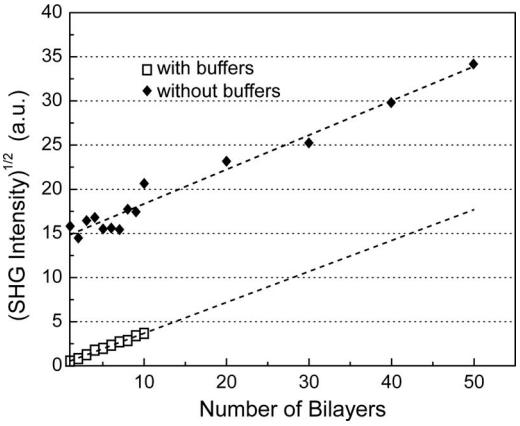

Fig. 4. Square root of the SHG intensity from PAH/PCBS ISAM films as a function of thickness with and without ten NLO-inactive PAH/PAA buffers. The addition of the buffers eliminates the interface contribution (y intercept) to the SHG signal. The lines are a guide to the eye.

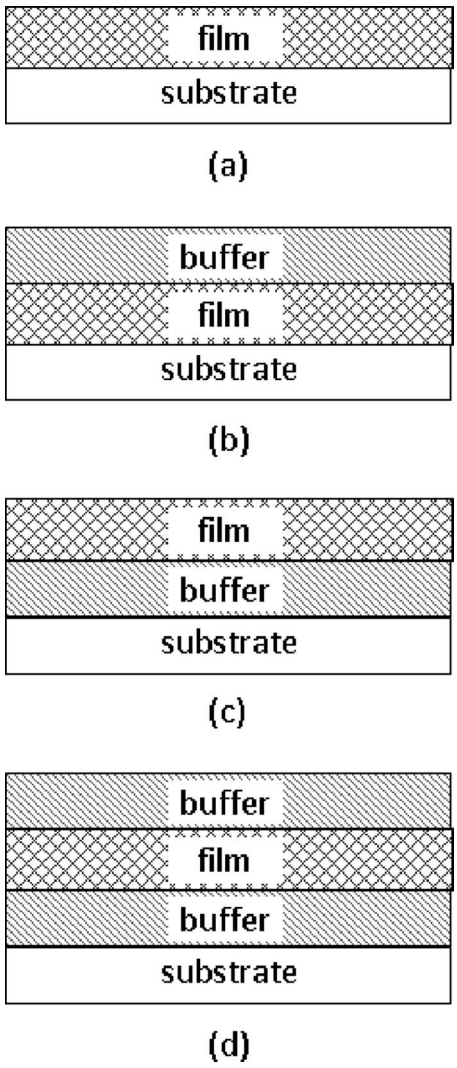

Fig. 5. Schemes of the four different configurations: (a) film only, (b) film–buffer, (c) buffer–film, (d) buffer–film–buffer. The films are NLO-active 1-bilayer or 3-bilayer PAH/PCBS or PAH/PB films, while each buffer consists of 10 bilayers of NLO-inactive PAH/PAA.

This is likely so because the PAH/PAA buffer layer has a larger surface charge density than the bare glass surface and will therefore attract a larger quantity of PAH for the first layer of the NLO-active film than the bare glass. The differences in chromophore density are accounted for by normalizing the SHG data with absorbance in order to compare the NLO characteristics of the different buffer/film configurations. The 3-bilayer films exhibit stronger SHG signal than the 1-bilayer films and the PAH/PB films exhibit stronger SHG than the PAH/PCBS films, as expected. Most of the remainder of this discussion is therefore based on Figs. 6(e) and 6(f).

First, interface SHG is indeed dominant in these films, as is evidenced by the much smaller signal from the buffer–film–buffer samples compared to the film-only samples. The reduction of the square root of the SHG intensity is 62% and 47% in the 1- and 3-bilayer PAH/PCBS films, and 78% and 80% in the 1- and 3-bilayer PAH/PB films, respectively. It is interesting to note that the reduction is greatest in the PB-based films, demonstrating that

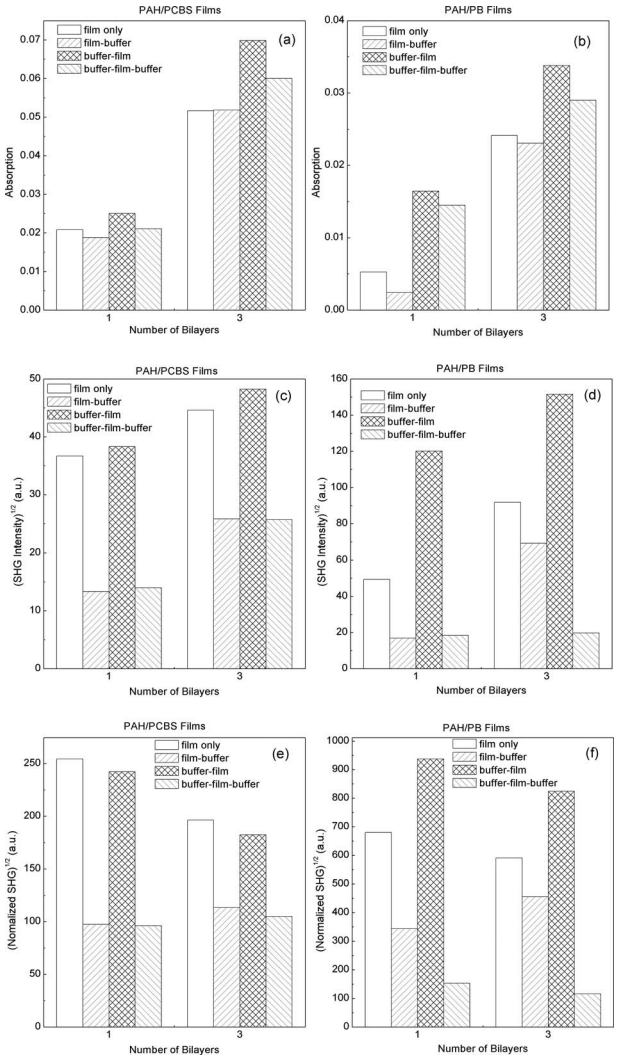

Fig. 6. Linear (absorption) and nonlinear (SHG) optical properties of films with or without buffer layers in the four different film/buffer combinations sketched in Fig. 3. (a), (b) Film absorption. (c), (d) Square root of SHG intensity. (e), (f) Square root of SHG intensity divided by absorption; used as a figure of merit of film performance.

the interface is even more important in these films than in conventional ISAM films.

Second, we can quantify the importance of the interface between film and air by comparing the SHG signal from the film-only samples to the corresponding film–buffer samples and also by comparing the signal from the buffer–film samples to the buffer–film–buffer samples. In all cases, removing the air interface results in a substantial reduction in the normalized SHG signal, ranging form 23% to 86%. It appears that the air interface is the dominant contribution to the SHG signal in most if not all cases studied here.

Third, the NLO properties of the glass–film interface are responsible for any differences between the film-only and buffer–film samples and between the film–buffer and buffer–film–buffer samples. In the PAH/PCBS films, these differences are small, and we conclude that the glass interface does not contribute significantly to the NLO properties of these samples. The situation is more complex for the PAH/PB films. There is a significant drop-off in signal from the film–buffer to the buffer–film–buffer configurations, consistent with an important contribution to the SHG from the glass interface. By contrast, the signal is actually larger in the buffer–film sample than in the film-only sample. This means that the SHG fields from the two interfaces must have opposite phase, leading to a partial cancellation when they are both present. The bulk SHG is too weak for us to be able to assign it a phase based on the results shown in Fig. 6, but the minimum in the SHG intensity from the unmodified PAH/PB plot in Fig. 3 indicates that the bulk SHG must be out of phase with the dominant interface SHG contribution, which is from the air interface.

Based on the above discussion, we can extract approximate quantitative values for interface-$\chi^{(2)}$ for both kinds of films. We model the effective $\chi^{(2)}$ value of each film as

$$\chi^{(2)}_{\text{eff}} = g + a + \gamma b l, \tag{1}$$

where g and a are the interface $\chi^{(2)}$ values of the glass and air interfaces, γ is the absorptivity of the films at 365 nm for PCBS films and 460 nm for PB films, and b is a materials parameter chosen such that γb is the bulk $\chi^{(2)}$ of the film. l is the thickness of the film, taken to be 1.17 nm per bilayer for the PAH/PCBS films [3] and 0.57 nm per bilayer for the PAH/PB films [1]. The values for γ are read from the data in Figs. 6(a) and 6(b), while the $\chi^{(2)}_{\text{eff}}$ values are proportional to the square root of the SHG intensities given in Figs. 6(c) and 6(d). For each material system, the parameters a, g, and b are found with a least-square fit to the data. All parameters are assumed positive, expect for those PAH/PB films where the air interface is unbuffered, where both a and $\chi^{(2)}_{\text{eff}}$ are taken to be negative.

Since systematic errors are likely to be fairly large, we use +100%/−50% as a normative error rather than the smaller error produced by the least-square fit. By comparing the data to the SHG signal from a known reference, a 68 bilayer PS-119/PAH ISAM film that has maintained a constant value of thickness and second-order susceptibility over the past 10 years [2], the results of the fit can be scaled to yield the values for interface and bulk $\chi^{(2)}$ that are listed in Table 2. Note that interface and bulk $\chi^{(2)}$ have different dimensions, so the values given for each are not directly comparable to each other.

The values obtained through the fit are consistent with the qualitative discussion above. For example, $g \ll a$ for the PAH/PCBS film, but not for the PAH/PB film. Bulk $\chi^{(2)}$ is an order of magnitude larger for PAH/PB compared to PAH/PCBS, while the total interface $\chi^{(2)}$ is only about three times as big.

As previously mentioned, the fact that NP-PAH/PB films have lower NLO efficiencies than NP-PAH/PCBS could be explained by a greater fragility of the air interface in the PAH/PB films. This notion is supported by the data plotted in Fig. 7, where SHG efficiency is plotted as a function of film thickness for freshly made PAH/PB films and for films that are a few months old. The aged films show small NLO efficiencies for the thinnest films and attain the minimum in SHG efficiency at a smaller film thickness, consistent with a lower value for interface $\chi^{(2)}$

Table 2. Effective $\chi^{(2)}$ Values for PAH/PCBS and PAH/PB Films as Derived by Least-squared Fit from the Data Compared to Bulk $\chi^{(2)}$ Values from a Single ISAM Bilayer[a]

	PAH/PCBS Film			PAH/PB Film		
	Air (a)	Glass (g)	Bulk (γb)	Air (a)	Glass (g)	Bulk (γb)
$\chi^{(2)}_{\text{eff}}$ (esu)	2.4×10^{-15}	0.4×10^{-15}	5×10^{-9}	-14×10^{-15}	5×10^{-15}	34×10^{-9}

[a]Note that dimension of bulk $\chi^{(2)}$ is that of hyperpolarizibility per cm^3, while interface $\chi^{(2)}$ is measured in hyperpolarizibility per cm^2, so the values in the two cases are not directly comparable.

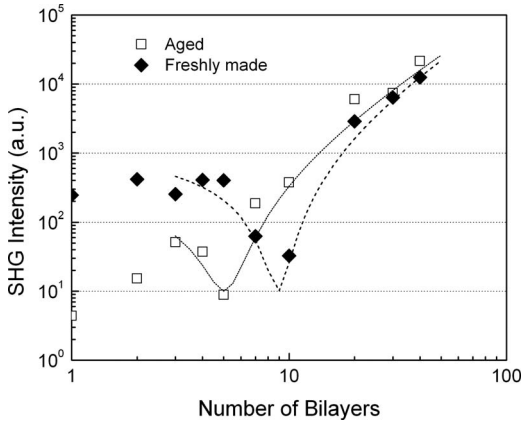

Fig. 7. Comparison of SHG signal from freshly made PAH/PB HCISAM film with the signal from films that are several months old. For the aged films, the SHG intensity is smaller from the thinnest films, and the minimum in the signal is shifted towards lower film thickness. The lines are mainly guides to the eye, as no formal fittings have been attempted to the data. However, the lines represent the expected functional dependence of a constant interface SHG out of phase with a bulk SHG that varies as the square of the number of bilayers.

in the older films. It is important to note that the difference between the fresh and aged films is largest for the thinnest films and becomes increasingly negligible as the number of bilayers is increased. This indicates that it is the interfaces that are undergoing change while the order of the bulk remains quite stable. The greater sensitivity of the PAH/PB film interface is possibly related to the manner in which it is fabricated. In the conventional PAH/PCBS films, the NLO chromophores are already present as side groups on the polymer during the LbL adsorption process, and the chain can assume a configuration that minimizes free energy, including the contributions from the chromophores. For PAH/PB films, the chromophores are grafted onto the PAH backbone after it has already assembled on the surface in a configuration that does not take into account the presence of the PB chromophores. It is then reasonable that the PAH/PB surfaces are more susceptible to rearrangement since they likely to be farther from an energetic minimum. In this context it is interesting to again note that the $\chi^{(2)}$ of the PAH/PB surface has the opposite sign of the bulk, which would seem to indicate that the topmost polymer layer undergoes substantial rearrangement as subsequent layers are deposited. Further investigations are needed to elucidate this process further.

5. CONCLUSION

In investigating plasmonic enhancement of $\chi^{(2)}$ values in thin ISAM films, we have found that the enhancement primarily stems from interface $\chi^{(2)}$. Thus, bulk $\chi^{(2)}$ values cannot be used to predict the NLO properties of a film enhanced by plasmonic nanoparticles for two reasons. First, the NLO response of the interface is not necessarily related to the corresponding bulk response. Second, the interfaces in different materials may be affected differently by the addition of metallic nanoparticles. Our comparison of PAH/PCBS ISAM films with PAH/PB HCISAM films is a good example of both effects. $\chi^{(2)}$ values of the film–air interface have the same sign as bulk $\chi^{(2)}$ in PAH/PCBS but the opposite sign in PAH/PB. And even though interface $\chi^{(2)}$ is substantially smaller in PAH/PCBS than in PAH/PB, plasmonically enhanced PAH/PCBS films exhibit the strongest NLO response. This may be because the structure of PAH/PB films makes its interface more susceptible to disruption by the nanoparticle deposition process, even though its bulk properties are as stable as the PAH/PCBS films.

The results suggest that the best route forward in plasmonic enhancement of NLO properties may lie in direct attachment of nonlinear chromophores to the surface of metal nanoparticles. Techniques for attaching molecules to noble metals by way of functional groups such as thiols [18,19] or dithiocarbamates [20,21] are well developed and understood, so such an approach gives the greatest possible control over all aspects of the interface while completely eliminating the less important bulk from the problem.

Our observations also have ramifications for the plasmonic enhancement of other optical phenomena such as surface-enhanced Raman scattering (SERS) [22–24] or high-order frequency generation [25–27]. In particular, one cannot assume that hyperpolarizabilities and Raman cross sections seen in bulk samples are unchanged when optically active species are absorbed onto metal nanoparticles. The well-known “chemical” component of the SERS enhancement is an example of this [22,28]. However, this effect is particularly large for second-order NLO effects since they depend on the existence of large-scale order. As we have seen, this order can sometimes be easily disrupted by the presence or deposition of metal nanoparticles, significantly reducing the nonlinear effects.

ACKNOWLEDGMENTS

This work was supported in part by a grant from the National Science Foundation (NSF) under agreement CBET-0756693 and by the Institute for Critical Technology and Applied Science (ICTAS). The authors acknowledge Peter Vikesland for use of the UV-Vis-NIR spectrophotometer.

REFERENCES

1. A. Garg, R. M. Davis, C. Durak, J. R. Heflin, and H. W. Gibson, "Polar orientation of a pendant anionic chromophore in thick layer-by-layer self-assembled polymeric films," J. Appl. Phys. **104**, 053116 (2008).
2. J. R. Heflin, C. Figura, D. Marciu, Y. Liu, and R. O. Claus, "Thickness dependence of second-harmonic generation in thin films fabricated from ionically self-assembled monolayers," Appl. Phys. Lett. **74**, 495–497 (1999).
3. J. R. Heflin, M. T. Guzy, P. J. Neyman, K. J. Gaskins, C. Brands, Z. Wang, H. W. Gibson, R. M. Davis, and K. E. Van Cott, "Efficient, thermally stable, second-order nonlinear optical response in organic hybrid covalent/ionic self-assembled films," Langmuir **22**, 5723–5727 (2006).
4. K. E. Van Cott, M. T. Guzy, P. J. Neyman, C. Brands, J. R. Heflin, H. W. Gibson, and R. M. Davis, "Layer-by-layer deposition and ordering of low-molecular-weight dye molecules for second-order nonlinear optics," Angew. Chem., Int. Ed. Engl. **41**, 3236–3238 (2002).
5. G. Decher, "Fuzzy nanoassemblies: toward layered polymeric multicomposites," Science **277**, 1232–1237 (1997).
6. K. Chen, C. Durak, J. R. Heflin, and H. D. Robinson, "Plasmon-enhanced second-harmonic generation from ionic self-assembled multilayer films," Nano Lett. **7**, 254–258 (2007).
7. C. L. Haynes and R. P. Van Duyne, "Nanosphere lithography: a versatile nanofabrication tool for studies of size-dependent nanoparticle optics," J. Phys. Chem. B **105**, 5599–5611 (2001).
8. T. R. Jensen, M. D. Malinsky, C. L. Haynes, and R. P. Van Duyne, "Nanosphere lithography: tunable localized surface plasmon resonance spectra of silver nanoparticles," J. Phys. Chem. B **104**, 10549–10556 (2000).
9. E. Hao and G. C. Schatz, "Electromagnetic fields around silver nanoparticles and dimers," J. Phys. Chem. **120**, 357–366 (2004).
10. K. Kneipp, Y. Wang, H. Kneipp, L. T. Perelman, I. Itzkan, R. Dasari, and M. S. Feld, "Single molecule detection using surface-enhanced Raman scattering (SERS)," Phys. Rev. Lett. **78**, 1667–1670 (1997).
11. S. Nie and S. R. Emory, "Probing single molecules and single nanoparticles by surface-enhanced Raman scattering," Science **275**, 1102–1106 (1997).
12. H. A. Clark, P. J. Campagnola, J. P. Wuskell, A. Lewis, and L. M. Loew, "Second-harmonic generation properties of fluorescent polymer-encapsulated gold nanoparticles," J. Am. Chem. Soc. **122**, 10234–10235 (2000).
13. K. Tsuboi, S. Abe, S. Fukuba, M. Shimojo, M. Tanaka, K. Furuya, K. Fujita, and K. Kajikawa, "Second-harmonic spectroscopy of surface immobilized gold nanospheres above a gold surface supported by self-assembled monolayers," J. Phys. Chem. B **125**, 174703 (2006).
14. W. Fan, S. Zhang, N. C. Panoiu, A. Abdenour, S. Krishna, R. M. Osgood, K. J. Malloy, and S. R. J. Brueck, "Second-harmonic generation from a nanopatterned isotropic nonlinear material," Nano Lett. **6**, 1027–1030 (2006).
15. M. Ishifuji, M. Mitsuishi, and T. Miyashita, "Bottom-up design of hybrid polymer nanoassemblies elucidates plasmon-enhanced second-harmonic generation from nonlinear optical dyes," J. Am. Chem. Soc. **131**, 4418–4424 (2009).
16. W. Kern, "Purifying Si and SiO_2 surfaces with hydrogen peroxide," Semicond. Int. **7**, 94–99 (1984).
17. B. G. Prevo and O. D. Velev, "Controlled, rapid deposition of structured coatings from micro- and nanoparticle suspensions," Langmuir **20**, 2099–2107 (2004).
18. C. D. Bain, E. B. Troughton, Y. T. Tao, J. Evall, G. M. Whitesides, and R. G. Nuzzo, "Formation of monolayer films by the spontaneous assembly of organic thiols from solution onto gold," J. Am. Chem. Soc. **111**, 321–335 (1989).
19. A. C. Templeton, M. P. Wuelfing, and R. W. Murray, "Monolayer protected cluster molecules," Acc. Chem. Res. **33**, 27–36 (2000).
20. Y. Zhao, W. Perez-Segarra, Q. C. Shi, and A. Wei, "Dithiocarbamate assembly on gold," J. Am. Chem. Soc. **127**, 7328–7329 (2005).
21. M. C. Tong, W. Chen, J. Sun, D. Ghosh, and S. W. Chen, "Dithiocarbamate-capped silver nanoparticles," J. Phys. B **110**, 19238–19242 (2006).
22. W. E. Doering and S. M. Nie, "Single-molecule and single-nanoparticle SERS: examining the roles of surface active sites and chemical enhancement," J. Phys. B **106**, 311–317 (2002).
23. D. A. Genov, A. K. Sarychev, V. M. Shalaev, and A. Wei, "Resonant field enhancements from metal nanoparticle arrays," Nano Lett. **4**, 153–158 (2003).
24. A. J. Haes and R. P. Van Duyne, "A nanoscale optical blosensor: sensitivity and selectivity of an approach based on the localized surface plasmon resonance spectroscopy of triangular silver nanoparticles," J. Am. Chem. Soc. **124**, 10596–10604 (2002).
25. T. Y. F. Tsang, "Surface-plasmon-enhanced third-harmonic generation in thin silver films," Opt. Lett. **21**, 245–247 (1996).
26. D. Yelin, D. Oron, S. Thiberge, E. Moses, and Y. Silberberg, "Multiphoton plasmon-resonance microscopy," Opt. Express **11**, 1385–1391 (2003).
27. M. Lippitz, M. A. van Dijk, and M. Orrit, "Third-harmonic generation from single gold nanoparticles," Nano Lett. **5**, 799–802 (2005).
28. A. Campion and P. Kambhampati, "Surface-enhanced Raman scattering," Chem. Soc. Rev. **27**, 241–250 (1998).